Swash zone boundary conditions derived from optical remote sensing of swash zone flow patterns

H. E. Power,[1] R. A. Holman,[2] and T. E. Baldock[1]

Received 13 October 2010; revised 27 January 2011; accepted 3 February 2011; published 15 June 2011.

[1] Optical remote sensing is used to measure flow patterns in the swash zone. Timestack images are analyzed to measure the asymmetry and the relative duration of the inflow into the swash zone. This varies significantly between individual swashes, contrary to the classical analytical swash model for runup induced by bores, which predicts a similar flow pattern for all events. For swash forced by breaking bores, the gradient of the x-t locus of flow reversal varies over a wide range and flow reversal can occur simultaneously across the whole swash zone. This variation of the gradient of the locus of flow reversal in x-t space can be parameterized in terms of a single free variable in recent solutions to the nonlinear shallow water equations, which fully defines the swash boundary inflow condition. Consistent with the theory, the horizontal runup, the swash period, and the swash similarity parameter were observed to be independent of the swash inflow conditions but the flow asymmetry is not. Only a weak correlation was observed between the swash boundary condition and the Iribarren number and beach slope. Conversely, the analysis suggests that the degree of swash-swash interaction does influence the swash boundary condition and the resulting internal flow kinematics. The variation in inflow conditions is expected to influence the magnitudes of the velocity moments within the swash zone and therefore sediment transport rates.

Citation: Power, H. E., R. A. Holman, and T. E. Baldock (2011), Swash zone boundary conditions derived from optical remote sensing of swash zone flow patterns, *J. Geophys. Res.*, *116*, C06007, doi:10.1029/2010JC006724.

1. Introduction

[2] Swash zone dynamics are a fundamental component of the forcing for the beach system. The swash zone links the terrestrial and marine environments and is an important mechanism of sediment exchange between the surf zone and subaerial beach [*Masselink and Puleo*, 2006]. However, sediment transport is generally poorly predicted, particularly accretionary conditions [*Elfrink and Baldock*, 2002; *Masselink and Puleo*, 2006]. To address this, a recent focus of study has been the advection of sediment into the swash zone, which balances the natural asymmetry of the swash hydrodynamics that favor the export sediment from the swash zone [*Hughes et al.*, 1997; *Puleo et al.*, 2000; *Pritchard and Hogg*, 2005; *Masselink and Puleo*, 2006]. Both the quantity of advected sediment and the flow asymmetry depend on the flow characteristics, particularly the duration of the inflow and the time at which the flow reverses between uprush and backwash. In violation of the classical *Shen and Meyer* [1963] model, observations show considerable scatter or variability of these parameters on a swash-by-swash basis [*Raubenheimer*, 2002; *Puleo et al.*, 2003; *Hughes and Baldock*, 2004; *Houser and Barrett*, 2010]. *Shen and Meyer* [1963] found that the swash is independent of the variability of the bore conditions in the inner surf zone, i.e., the solution depends on a fixed seaward boundary condition and initial shoreline velocity. However, *Guard and Baldock* [2007] showed that different boundary conditions provide alternative solutions of the nonlinear shallow water wave equations. These different boundary conditions describe different forcing or inflow conditions at the seaward swash boundary, and allow the solutions to describe variability in the internal flow field for different swash events. In nondimensional form, the solutions are controlled by a single free boundary condition parameter, k, which controls the mass and momentum flux into the swash zone. In dimensional form, or physical parameters, the characteristics of the flow are controlled by the wave or bore height, wave or bore period, waveshape and asymmetry, and incident velocity [*Elfrink and Baldock*, 2002]. In addition, the inner surf conditions experienced by the incident bore depend on swash-swash interactions, wave-induced currents and long waves, all of which have the potential to influence the momentum flux into the swash zone.

[3] The *Shen and Meyer* [1963] model is a special solution to the nonlinear shallow water (NLSW) equations [*Peregrine and Williams*, 2001; *Pritchard and Hogg*, 2005], and represents an asymptotic description of the flow close to the wave tip for a single and specific boundary condition. It has been shown to closely approximate the shoreline motion in the swash zone, particularly if frictional effects at the wave tip are included

[1]School of Civil Engineering, University of Queensland, St Lucia, Queensland, Australia.
[2]College of Oceanic and Atmospheric Sciences, Oregon State University, Corvallis, Oregon, USA.

0148-0227/11/2010JC006724

[*Hughes*, 1995; *Baldock and Holmes*, 1999; *Puleo and Holland*, 2001]. However, it does not accurately describe the internal hydrodynamics, i.e., the flow depth and velocity [*Baldock et al.*, 2005; *Guard and Baldock*, 2007]. Further, the apparent scatter in the asymmetry between uprush and backwash flow durations, as widely observed in the field and laboratory [*Kemp*, 1975; *Raubenheimer et al.*, 1995; *Baldock and Holmes*, 1997; *Masselink and Hughes*, 1998; *Raubenheimer*, 2002], is not consistent with the Shen-Meyer solution. On fine-grained sandy beaches, these differences are not likely to be a result of friction or infiltration, which primarily influence the flow close to the leading edge, i.e., the shoreline motion. For example, *Packwood* [1983] shows negligible influence from infiltration during runup on fine and medium sand beaches. In addition, the classical solution is hydrodynamically similar for all swash events and simply scales on the runup amplitude [*Peregrine and Williams*, 2001]; i.e., after the initial bore collapse, the internal properties of the swash are independent of the conditions at the seaward swash boundary irrespective of the surf zone conditions. This is inconsistent with a wide range of observations of variability in the hydrodynamics, sediment transport and morphological change, where the latter also varies on a swash-by-swash basis [*Waddell*, 1976; *Baldock*, 2009; *Turner et al.*, 2009].

[4] The Shen-Meyer solution neglects the mass and momentum of the flow behind the incident bore front, and hence any variability in these physical parameters as a result of variability in the inner surf conditions. Recognizing this, *Guard and Baldock* [2007] developed new numerical solutions to the nonlinear shallow water equations that allow variable swash boundary conditions. The variable swash boundary conditions do not affect the shoreline motion, which does not differ from that predicted by *Shen and Meyer* [1963]; only the internal kinematics, in particular the flow asymmetry and time of flow reversal, are different. The physical cause for the different flow behavior is the inclusion of the mass and momentum of the flow behind the incident bore front, i.e., a more sustained inflow across the seaward boundary of the swash zone.

[5] The importance of the swash zone boundary condition was illustrated by *Baldock et al.* [2005], who showed that real swash overtopping volumes were much greater than predicted by the Shen-Meyer model [cf. *Peregrine and Williams*, 2001] and by *Pritchard* [2009] who demonstrated that sediment transport predictions differ between the Shen-Meyer model [cf. *Pritchard and Hogg*, 2005] and the more recent solutions. Differences in asymmetry in the flow field between different swash events are likely to lead to differences in net sediment transport directions [*Elfrink and Baldock*, 2002; *Pritchard*, 2009]. Indeed, *Houser and Barrett* [2010] show differences between periods of accretion or erosion of the beach face could be separated by the different relative time of flow reversal in the swash zone. However, while the field data of *Masselink and Hughes* [1998], *Raubenheimer* [2002], *Hughes and Baldock* [2004], and H*ouser and Barrett* [2010] suggest that the time of flow reversal is quite variable and different from the behavior predicted by the Shen-Meyer model, this has not been related to the different possible solutions of the nonlinear shallow water equations for natural conditions. Further, the variation of the incoming mass and momentum for different surf and swash conditions has not been identified and quantified in the field. Identifying such variations is important for improved wave by wave and stochastic descriptions of overtopping of structures and dunes, and for modeling the sediment flux across the surf-swash boundary.

[6] This paper addresses this issue and presents the first comprehensive data set showing the variation in the swash inflow conditions on real beaches and that this variation is consistent with the recent solutions of the NLSW equations. The data suggest that this is the reason why natural bore induced swash is different from the Shen-Meyer model, instead of being a result of other processes which might make the swash deviate from the Shen-Meyer solution (e.g., the effects of infiltration and friction). We also show the development of a new application of remote sensing to provide quantitative data which can be directly compared to numerical model results. Section 2 outlines the numerical model and illustrates the importance of the boundary condition for the swash hydrodynamics. Section 3 describes the methods of data collection, the preprocessing required to obtain timestack images and the method used to identify and verify the locus of flow reversal and the boundary condition parameter, k, for individual swash events. The results of this analysis are presented in section 4 together with a statistical analysis of the relationship between k and various time-averaged offshore and individual wave characteristics. Section 5 presents a discussion of the data and illustrates how remote measurements of the locus of flow reversal and k could be used to infer other parameters, particularly magnitudes of velocity moments. Final conclusions are outlined in section 6.

2. Swash Hydrodynamics Model

[7] The *Guard and Baldock* [2007] model solves a nondimensional form of the NLSW equations written as

$$\begin{aligned} \frac{\partial h}{\partial t} + \frac{\partial (uh)}{\partial x} &= 0 \\ \frac{\partial u}{\partial t} + u\frac{\partial u}{\partial x} + \frac{\partial h}{\partial x} + 1 &= 0, \end{aligned} \tag{1}$$

where x is the dimensionless cross-shore distance, t is the dimensionless time, h is the dimensionless water depth measured perpendicular to the slope, and u is the dimensionless flow velocity [*Peregrine and Williams*, 2001]. These parameters are related to the dimensional variables as follows:

$$x = \frac{\sin(\beta_{sw})x^*}{a}, t = (\sin\beta_{sw})t^*\sqrt{\frac{g}{a}}, h = \frac{(\cos\beta_{sw})h^*}{a}, u = \frac{u^*}{\sqrt{ga}}, \tag{2}$$

where * denotes dimensional variables, β_{sw} is angle of the beach face in the swash zone, g is the acceleration due to gravity, and $2a$ is the vertical excursion of the undisturbed swash. Substituting for the nondimensional shallow water wave speed, $c = \sqrt{h}$, (1) may be rearranged to obtain

$$\begin{aligned} \left(\frac{\partial}{\partial t} + (u+c)\frac{\partial}{\partial x}\right)(u + 2c + t) &= 0 \\ \left(\frac{\partial}{\partial t} + (u-c)\frac{\partial}{\partial x}\right)(u - 2c + t) &= 0. \end{aligned} \tag{3}$$

Introducing the characteristic variables $\alpha(x, t)$ and $\beta(x, t)$ gives

$$\frac{d}{dt}\alpha = 0 \text{ on } \frac{dx}{dt} = u + c, \tag{4}$$

$$\frac{d}{dt}\beta = 0 \text{ on } \frac{dx}{dt} = u - c, \tag{5}$$

where

$$\begin{aligned} \alpha(x,t) &= u + 2c + t \\ \beta(x,t) &= u - 2c + t. \end{aligned} \tag{6}$$

The solutions and model results are controlled by the value of $\alpha(t)$ on the seaward swash boundary. The Shen-Meyer solution corresponds to a constant value of $\alpha = 2$, which results in a very thin swash. *Guard and Baldock* [2007] allowed the value of the characteristic variable on the seaward boundary, α, to vary over time, such that

$$\alpha(t) = 2 + kt, \tag{7}$$

where k is a constant for each individual swash and $k = 0$ corresponds to the Shen-Meyer solution. Choosing $k \neq 0$ allows $\alpha(t)$ to vary through time, which is the fundamental difference introduced by *Guard and Baldock* [2007]. An analytical form of these solutions was later developed by *Pritchard et al.* [2008], verifying the previous numerical scheme. Initially k was expected to lie in the range $0 < k < 1$, where $k = 1$ corresponds to conditions representative of uniform incident bores. Hence, the Shen-Meyer solution is identical for all swash events, but the Guard-Baldock model allows different hydrodynamics for different individual swash events by specification of different values for the boundary condition parameter k. *Baldock and Hughes* [2006] presented photographs of incident bores where the water surface elevation behind the bore front is horizontal, consistent with near uniform bore conditions. The solutions in nondimensional form are independent of beach slope, swash period and runup amplitude. It is therefore important to note that values of k derived from observations should therefore *not* be dependent on swash beach slope, swash period or runup amplitude, although beach slope does influence the inner surf zone conditions.

[8] Varying the boundary conditions on the seaward boundary, corresponding to varying $\alpha(t)$ on the incoming characteristics, results in deeper and less asymmetric swash flows than those predicted by the Shen-Meyer solution. The physical significance of the characteristic values α and β is shown by writing

$$u = \frac{\alpha + \beta - 2t}{2} \quad c = \frac{\alpha - \beta}{4}, \tag{8}$$

which gives the nondimensional volume flux, q, and momentum flux, M, per unit length of wave crest as

$$\begin{aligned} q = uh &= \frac{1}{32}(\alpha + \beta - 2t)(\alpha - \beta)^2 \\ M = u^2h &= \frac{1}{64}(\alpha + \beta - 2t)^2(\alpha - \beta)^2. \end{aligned} \tag{9}$$

The physical interpretation is that solutions for different $\alpha(t)$ correspond to different mass and momentum flux across the seaward boundary.

[9] By varying k, and consequently $\alpha(t)$, the incoming mass and momentum fluxes at the seaward boundary can differ for each swash event, which results in different flows within the swash zone. Increases in k represent more sustained inflow conditions and lead to solutions that have a later flow reversal, increased depths in the swash, and a more symmetric velocity field between uprush and backwash. Figure 1 shows (x, t) contour plots of cross-shore velocities, u, for four values of k. The locus of flow reversal (contour of $u = 0$) varies significantly for solutions between $k = 0$ and $k = 1$; at the seaward swash boundary flow reversal occurs after one quarter of the whole swash cycle for $k = 0$, whereas for $k = 1$ flow reversal occurs approximately halfway through the swash cycle. Thus, the specified boundary condition, as defined by k, controls the overall asymmetry of the flow field. Therefore, the Guard-Baldock model shows that differences between observations of swash hydrodynamics and the Shen-Meyer model do not have to be attributed to the effects of infiltration or friction; real bore induced swash can be fundamentally different to the Shen-Meyer model as a result of the inflow conditions at the seaward boundary.

[10] Full numerical solutions of the NLSW equations also provide good estimates of the swash hydrodynamics [*Hibberd and Peregrine*, 1979; *Kobayashi et al.*, 1989; *Raubenheimer*, 2002], but do not illustrate the influence of the swash boundary conditions in such a transparent manner, nor have they been used to investigate the variation in flow asymmetry between different swash events on natural beaches or in laboratory studies. Experimental laboratory data suggests that $0.8 < k < 1.4$ is appropriate for swash forced by solitary long bores [*Guard and Baldock*, 2007; *Baldock and Peiris*, 2010]. However, while the field data of *Hughes and Baldock* [2004] and *Houser and Barrett* [2010] suggest that $k > 0$ on natural beaches, there is no quantitative field data that demonstrates appropriate values for k for natural conditions.

3. Methods

[11] Remote sensing techniques, such as the use of video data, are becoming more common in coastal studies and techniques have advanced greatly in recent years [*Holman and Stanley*, 2007]. The key advantage of using remote sensing techniques is that they allow for the collection of large amounts of data relatively easily, and data can be obtained from a large spatial domain. Since the swash zone boundary (location of initial runup) varies for each and every wave, a very large and dense array of conventional fixed instrumentation would be required to measure the flow depth and flow velocity at the seaward swash boundary on a wave-by-wave basis. Optical remote sensing of the inner surf and swash zone region overcomes this difficulty automatically.

[12] This study utilizes video data obtained in the swash zone using the timestack method developed by *Aagaard and Holm* [1989]. Timestack images show cross-shore distance on the x axis and time on the y axis (e.g., Figure 2), and have previously been used to measure shoreline position through time, nearshore bathymetry, flow velocities and wave speeds

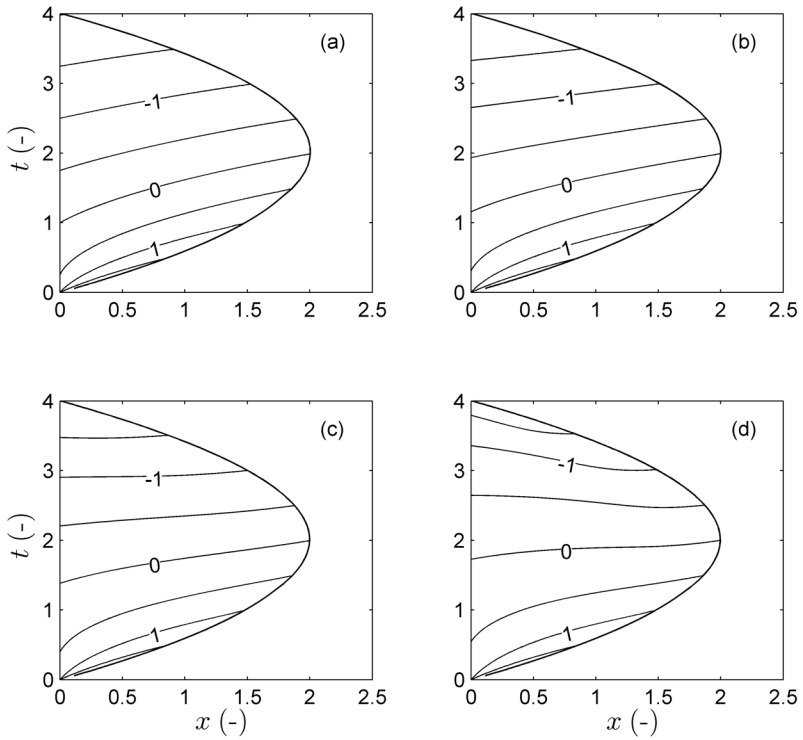

Figure 1. Contours of flow velocity and the locus of the position of horizontal flow reversal ($u = 0$ contour) across the swash zone for (a) $k = 0$, (b) $k = 1/3$, (c) $k = 2/3$, and (d) $k = 1$ given by *Guard and Baldock* [2007]. Flow characteristics are nondimensional corresponding to a nondimensional swash period of $T = 4$ and a nondimensional runup length of $x = 2$.

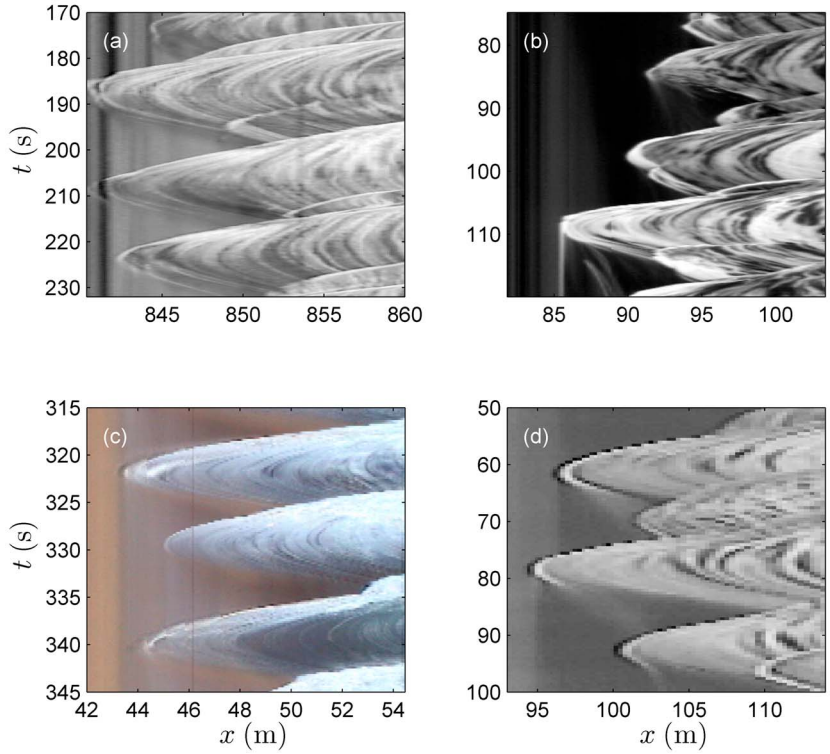

Figure 2. Examples of timestack images from (a) NCEX, (b) Duck on 17 October 2009 at 1345 UT, (c) Cabarita, (d) Duck on 18 April 2009 at 1540 UT.

Table 1. Location, Date, Number of Hours of Video Data Analyzed, Number of k Values Obtained, Beach Slope, Significant Offshore Wave Height, Average Offshore Wave Period, and Iribarren Number for Each Day of Video Data[a]

Location	Date	n	n_k	$\tan\beta$	H_o (m)	T_z (s)	ξ
Black's Beach, CA, USA	Sep-Dec 2003	0.03	5	0.027[b]	1.13	5.88	0.19
Brunswick Heads, NSW	24 Aug 2009	2	18	0.038	0.90	4.28	0.22
Cabarita Beach, NSW	12 Nov 2009	4	986	0.104	0.92	5.42	0.74
Duck, NC, USA	19 Mar 2003	0.28	17	0.064[b]	2.85	6.03	0.29
Duck, NC, USA	20 Mar 2003	0.28	23	0.064[b]	2.61	6.60	0.33
Duck, NC, USA	11 Apr 2003	0.28	18	0.064[b]	3.39	7.80	0.34
Duck, NC, USA	18 Apr 2003	0.28	30	0.064[b]	2.88	6.94	0.33
Duck, NC, USA	19 Apr 2003	0.28	32	0.064[b]	2.67	6.47	0.32
Duck, NC, USA	20 Apr 2003	0.28	21	0.064[b]	3.12	7.62	0.35
Duck, NC, USA	19 Sep 2009	0.26	31	0.064[b]	1.04	5.52	0.43
Duck, NC, USA	23 Sep 2009	0.17	11	0.064[b]	1.04	5.69	0.45
Duck, NC, USA	26 Sep 2009	0.26	35	0.064[b]	2.03	5.70	0.32
Duck, NC, USA	3 Oct 2009	0.09	4	0.064[b]	1.11	5.20	0.40
Duck, NC, USA	12 Oct 2009	0.26	48	0.064[b]	1.65	4.77	0.30
Duck, NC, USA	14 Oct 2009	0.26	57	0.064[b]	1.59	5.23	0.33
Duck, NC, USA	17 Oct 2009	0.26	34	0.064[b]	2.26	7.03	0.37
Duck, NC, USA	19 Oct 2009	0.26	21	0.064[b]	2.32	5.79	0.30
Duck, NC, USA	21 Oct 2009	0.26	56	0.064[b]	0.61	6.57	0.67
Duck, NC, USA	14 Nov 2009	0.26	22	0.064[b]	3.46	7.94	0.34
Duck, NC, USA	15 Nov 2009	0.17	7	0.064[b]	2.48	8.82	0.45
Duck, NC, USA	16 Nov 2009	0.17	2	0.064[b]	1.59	8.71	0.55
Duck, NC, USA	17 Nov 2009	0.26	13	0.064[b]	1.81	6.39	0.38
Duck, NC, USA	18 Nov 2009	0.26	21	0.064[b]	2.14	5.94	0.33
Duck, NC, USA	19 Dec 2009	0.26	22	0.064[b]	5.17	8.08	0.28
Duck, NC, USA	20 Dec 2009	0.26	19	0.064[b]	2.55	7.07	0.35
Duck, NC, USA	26 Dec 2009	0.26	21	0.064[b]	3.36	8.3	0.36
Duck, NC, USA	27 Dec 2009	0.26	22	0.064[b]	1.88	8.64	0.50
Moreton Island, Qld	7 Dec 2009	2.5	61	0.055	0.87	4.93	0.37
Moreton Island, Qld	8 Dec 2009	2	24	0.051	0.85	4.16	0.29
The Spit, Qld	11 Mar 2009	2	166	0.041	3.01	6.95	0.21
The Spit, Qld	12 Mar 2009	2	188	0.043	2.34	6.17	0.22
The Spit, Qld	11 Aug 2009	2	42	0.037	1.69	9.29	0.33
The Spit, Qld	9 Nov 2009	4	129	0.043	1.69	5.63	0.23
The Spit, Qld	10 Nov 2009	6	141	0.051	1.55	5.29	0.27
The Spit, Qld	11 Nov 2009	3	46	0.064	1.03	5.39	0.43

[a]Here n is number of hours of video data analyzed, n_k is number of k values obtained, $\tan\beta$ is beach slope, H_o is significant offshore wave height, T_z is average offshore wave period, and ξ is Iribarren number. All beaches are in Australia unless otherwise indicated.

[b]The beach slope listed is only a representative slope as profiles were not measured for every data set. Thus, in these cases Iribarren numbers are also only representative. For additional information on beach slopes at Duck, North Carolina, United States, see *Larson and Kraus* [1994].

[e.g., *Holland and Holman*, 1993; *Stockdon and Holman*, 2000; *Ranasinghe et al.*, 2004]. The locus of flow reversal, i.e., the $u = 0$ contour on Figure 1, appears clearly on high-quality timestack images of swash streak lines. The x-t gradient of the locus of flow reversal can then be directly quantified by the single boundary condition parameter, k, in the *Guard and Baldock* [2007] model.

3.1. Field Sites

[13] This study presents video data obtained from six different beaches on 34 different days (Table 1). Data from each day did not cover more than one individual tidal cycle (i.e., 12 h or less). The data were collected from a large range of beach types from reflective to dissipative [*Wright and Short*, 1984]. All beaches examined in this study are characterized by microtidal, swell dominated conditions, with the majority of data from beaches on the east coast of Australia. The remaining data were collected at Duck, North Carolina, United States, and a small amount of data was obtained from the ONR/NSF Nearshore Canyon Experiment (NCEX, see http://science.whoi.edu/users/elgar /NCEX/ncex.html) at Black's Beach, California, United States.

3.2. Data Collection and Preprocessing

[14] The data collected on the Australian beaches were obtained using a portable digital video camera situated on a headland, foredune, or berm, and focused on the swash zone. The real world coordinates of a cross-shore line within the field of view were determined by surveying markers placed in the swash zone. Using these data, timestacks were created by sampling frames from the video data at 5 Hz. Pixel intensity profiles were taken along a cross-shore profile from each image and stacked through time to make a timestack (e.g., Figure 2c).

[15] The data from Duck were collected using the ARGUS video imaging system. Video recordings were obtained and the location of a cross-shore profile line was computed using known geometric transformations [*Lippmann and Holman*, 1989]. Video images were sampled at 6.67 Hz (e.g., Figures 2b and 2d).

[16] Examples of timestacks with different resolutions are shown in Figure 2. Figures 2b and 2d were collected at Duck using the ARGUS system. These two images highlight the importance of high image resolution and high sampling frequency to create good quality timestacks. The sampling

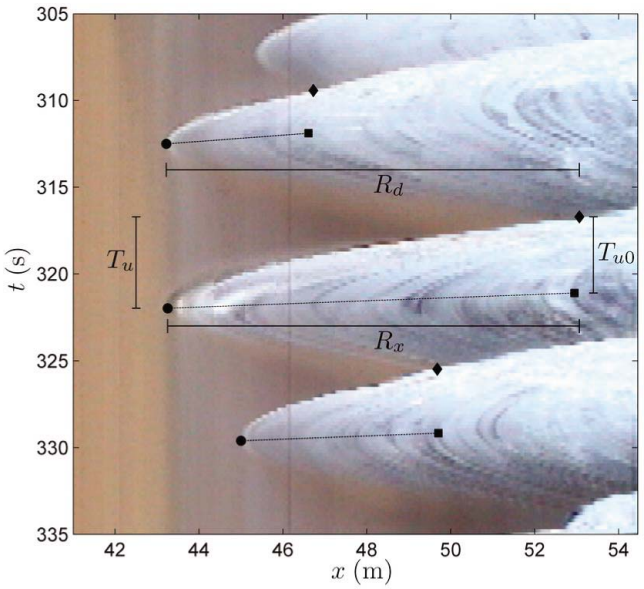

Figure 3. Example of a timestack image from Cabarita collected on 12 November 2009 (f_s = 5 Hz) showing the points that are required to calculate a value of k, the start of the uprush (solid diamonds), the maximum uprush point (solid circles), and a point in the wave where the flow velocity is zero (solid squares), and the line of flow reversal (dashed line). The swash uprush duration (T_u), the horizontal swash excursion length (R_x), the preceding rundown length (R_d), and the duration of the inflow at x = 0 (T_{u0}) are shown for the second wave.

frequency of these images is 2 and 6.67 Hz respectively. Figure 2a was collected during NCEX (see http://science.whoi.edu/users/elgar/NCEX/ncex.html) and is another example of a high-quality timestack; it has a sampling frequency of 6 Hz. Figure 2c is representative of the data sets collected in Australia using a portable digital video camera. All data collected in Australia was sampled at 5 Hz. The time of flow reversal at multiple cross-shore locations can be easily identified in the images, i.e., when the gradients of the streak lines change sign.

3.3. Calculation of *k*

[17] The time of flow reversal in both the swash and surf zones can be observed in the timestack images in Figure 2. Further examples for swash with different k values are shown in Figure 5. Only individual runup events forced by bores were analyzed. The maximum observed swash period was approximately 30 s, with over 99% of events having swash periods less than 20 s, i.e., within the sea swell frequency band. The u = 0 contour in Figure 1 is directly equivalent to the locus of flow reversal that can be observed from the streak lines in each of the events shown in Figure 2 (see also Figure 5). The timestacks were used to obtain the gradient of the line of the flow reversal in natural swash, i.e., where u = 0, and hence to derive values of k from the *Guard and Baldock* [2007] swash solution. This process can be completed by hand by locating three points for each swash event: the start of the uprush (x = 0, t = 0), the maximum uprush point ($x = x_{\max}$, $t = T_u$), and a point in the swash where the flow velocity is zero (Figure 3). The latter two points are used to obtain a line along which u = 0 and the former two points are used to obtain the uprush duration. Note that this technique assumes that the locus of flow reversal is a straight line in x-t space on the timestacks, which is not in perfect accord with the model solutions, but appears to be a robust approximation. The same assumption is made when calculating k from the model. Using the gradient of the locus of u = 0 and the x-t locations of the start of the uprush and maximum uprush, it is possible to back calculate a value for k for that individual swash event. This is done by calculating the length of the period of the inflow (onshore flow) at x = 0 (T_{u0}) relative to the uprush duration of the shoreline motion (T_u) (see Figure 3). To convert the observed ratio of the inflow and uprush duration into the model parameter k, the model was run for a range of k values to determine the following relationship between T_{u0}/T_u and k

$$k = 0.77e^{0.48T_{u0}/T_u} - 10.16e^{-4.67T_{u0}/T_u}, \quad (10)$$

which completes the analysis.

[18] For analysis of large data sets or near real time analysis of swash data it would be ideal to have a more automated process. A semiautomated algorithm to achieve this was developed by *Power et al.* [2009] but this requires high-quality images and timestacks which were not consistently available for this study. Therefore, to maintain consistency in the method applied, a manual analysis method was used for the analysis of all data sets presented here. The manual analysis method uses Matlab to automate the scrolling of the timestack image and automatically write the x-t coordinates of the groups of three points to a file, so the manual process is relatively quick, and simply involves selecting the required points on the image. Calculation of the gradient of the locus of flow reversal from the derived x-t coordinates, and the k values from the numerical model, is fully automatic.

[19] To ensure the manual analysis was not compromised due to user subjectivity, the manual data collection method was tested by three individuals (HP, TB, and SJ). Each individual analyzed the same 15 min of one timestack, collecting data for the same 54 waves, with two individuals repeating this twice (HP and TB). For each data set, k values were calculated to allow for direct comparison between k for each wave. Mean and standard deviations of k were also calculated for each data set. Root-mean-square errors (RMSE) calculated between the original data set (HP 1) and the other data sets ranged from 0.27 to 0.37 (Table 2) but means were not significantly different compared to the variation away from k = 0. To investigate what proportion of this error was due to image and screen resolution, three additional data sets were created by taking the original data set and adding random errors of ±1, ±2, and ±4 pixels (RE 1, RE 2, and RE 4) to each of the three points for each swash. This can lead to up to an RMSE of up to 0.38. In addition to this, the accuracy of the ability of one individual to repeatedly pick the same three individual points on the image was tested. For the image and screen resolution available for this study, the accuracy of the ability to pick the start of the uprush, the maximum uprush, and a flow reversal point on the same wave was ±2.5, ±1, and ±1.5 pixels, respectively. Random errors up to these maximum values were added to the

Table 2. Comparison of Mean and Standard Deviations of k and Root-Mean-Square Error Between Differently Sampled Data Sets[a]

Name of Data Set	$\overline{k}$	σ_k	RMSE Compared to Data Set HP 1
HP 1	0.56	0.28	–
HP 2	0.47	0.35	0.27
TB 1	0.64	0.42	0.36
TB 2	0.72	0.32	0.33
SJ	0.68	0.35	0.37
RE 1	0.54	0.31	0.11
RE 2	0.49	0.42	0.22
RE 4	0.57	0.42	0.38
RE T	0.55	0.33	0.18
HP O	0.46	0.31	0.24

[a]Here $\overline{k}$ is the mean and σ_k is the standard deviations of k.

original data set, providing a further data set (RE T). The RMSE for this test demonstrates that such errors account for half or more of the difference between data sets. Consequently, while the method is subject to inaccuracy in determining exact values of k for each individual swash, there is no obvious bias introduced by different users, and absolute exact values of k are not relevant to the remaining analysis. To ensure consistency, all data presented here were analyzed by HP.

[20] To determine if oblique swash could potentially bias the k values, a 15 min sample timestack was created along a profile line at an angle of 11.31° to shore normal. This oblique timestack has a corresponding timestack taken along a normal cross-shore profile line that is part of the total data set. In the same manner as the method described above, k values were collected for the same 54 waves on this oblique timestack (HP O) and compared to the original data set from the normal timestack (HP 1). The RMSE value for this comparison, 0.24, is almost equal to the RMSE introduced by image resolution and user accuracy, indicating that any errors due to oblique swash are not significant compared to the errors inherent in the image analysis process. In addition, a geometric analysis shows that this method of back calculating k is not affected by angle of the swash providing that the velocity of the foam creating the streaklines travels at fixed proportions of the velocity of the leading edge for that swash. In essence, the relative time between flow reversal and the time of the maximum uprush is not affected, and thus the x-t gradient of the locus of flow reversal is unchanged.

4. Results

4.1. The k Values for Individual Waves

[21] Selected histograms of k values derived from the data collected in Australia and at Duck are shown for the different beaches in Figure 4. It is clear that a wide range of values of k occur on natural beaches and that the mean value for k at all locations is significantly greater than zero (the Shen-Meyer swash boundary condition). The values of k are negatively skewed, indicating that there are comparatively more high values of k than low values. The histograms are similar for all three sites shown (and for those not shown). The total data set, consisting of 2393 individual waves, has a mean k value of 0.71 and is also strongly neg-

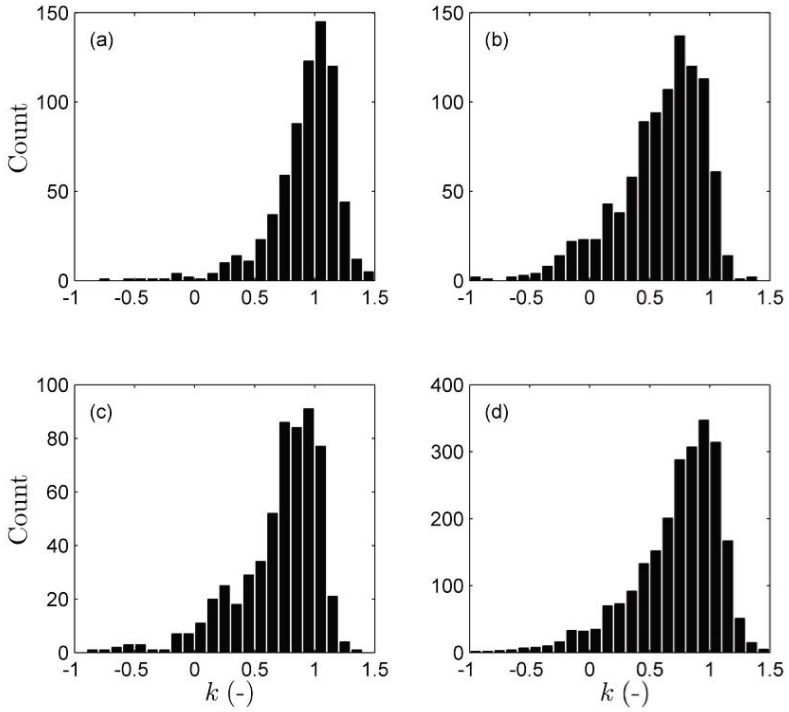

Figure 4. Histogram of all k values from (a) The Spit, Queensland, Australia, $n = 712$, $\overline{k} = 0.91$, skewness = −2.62; (b) Cabarita, $n = 986$, $\overline{k} = 0.57$, skewness = −2.41; (c) Duck, $n = 587$, $\overline{k} = 0.67$, skewness = −3.20; and (d) the k values from all the data sets combined, $n = 2393$, $\overline{k} = 0.71$, skewness = −2.57.

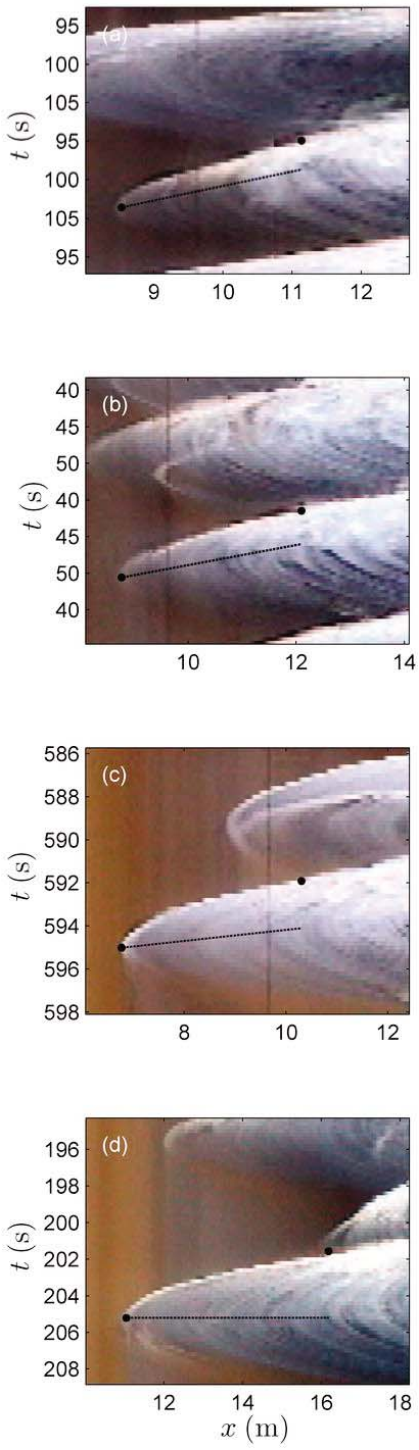

Figure 5. Example timestacks of waves from Cabarita with (a) $k = -0.38$, (b) $k = -0.015$, (c) $k = 0.71$, and (d) $k = 1.15$.

atively skewed, −2.57. Examples of portions of timestacks that show swashes with a range of k values from −0.38 to 1.15 are presented in Figure 5. Comparing the loci of flow reversal on Figure 5 with those shown on Figure 1 clearly illustrates the influence of the inflow conditions on the overall flow asymmetry, and the model captures this variability. Note that *Guard and Baldock* [2007] only considered $0 < k < 1$, but the model is valid outside this range, and it appears that real swash boundary conditions correspond to k values in the range −1 to 1.5. However, in the model, conditions for $k > 1.2$ represent swash where a bore forms in the backwash as a result of sustained high water levels at the seaward end of the swash zone, and the predicted flow characteristics in the vicinity of the bore are not necessarily representative of the true conditions. Nevertheless, high measured values of k correspond to flow reversal occurring after the time of maximum runup (see Figure 5d), which is very different to the Shen-Meyer solution.

[22] Figure 6 shows a comparison between measured values of k and three individual wave parameters: horizontal swash excursion (R_x), swash period (T), and the swash similarity parameter (ε) introduced by [*Miche*, 1951]

$$\varepsilon = \frac{a\omega^2}{g\beta_{sw}^2}, \tag{11}$$

where $2a$ is the vertical excursion which is calculated using $a = 0.5R_x \tan \beta_{sw}$. The swash period, T, was defined as twice the uprush duration (T_u) (see Figure 3), which is not necessarily exact, but T is only used to illustrate the range of swash duration and in the surf and swash similarity parameters. This approximation has no influence on the estimates of k. For monochromatic swash and a ballistic trajectory for the shoreline motion, $\varepsilon = 2.5$ represents the onset of swash saturation and the commencement of swash-swash interaction [*Baldock and Holmes*, 1999]. Figure 6 shows that there is no clear trend between k and R_x or T (Figures 6a and 6b). As noted previously, this is expected and consistent with the theoretical model, i.e., the value of k in the model does not influence either runup amplitude or period. No linear trend was observed between k and ε (Figure 6c); however, swashes with $\varepsilon \geq 2.5$ had a significantly larger mean k value ($\overline{k} = 0.98$) than swashes with $\varepsilon < 2.5$ ($\overline{k} = 0.69$; $\alpha = 0.01$, $t = 18.08$, d. f. = 672.23, $P = 0$). Additionally, negative values of k only occurred for swashes with $\varepsilon < 2.5$ (Figure 6c). While absolute k values are subject to some errors from the analysis technique, no bias occurs and hence these populations are unlikely to be significantly different. Overall, this suggests that the swash boundary condition and inflow period does not significantly affect either the runup length or the swash period, which is in agreement with the original Shen-Meyer model for the shoreline trajectory. However, k and ε show some (nonlinear) interdependency, which suggests that the degree of swash-swash interaction influences the inflow conditions and therefore the internal swash hydrodynamics (see also section 4.3). As evident from the Miche parameter, and as observed by *Guza and Bowen* [1976] and *Holland and Puleo* [2001], swash interaction is strongly dependent on beach slope and hence there is potential for strong hydromorphodynamic feedback in terms of the shoreline motion as a beach evolves. This analysis suggests that potential feedback also may extend to the inflow or swash boundary conditions.

4.2. Time-Averaged k Values

[23] To investigate any differences between the data from different locations and days, the correlation between k values and offshore wave parameters and beach slope was examined by comparing the means and standard deviations of k from all locations against five parameters. These are the offshore

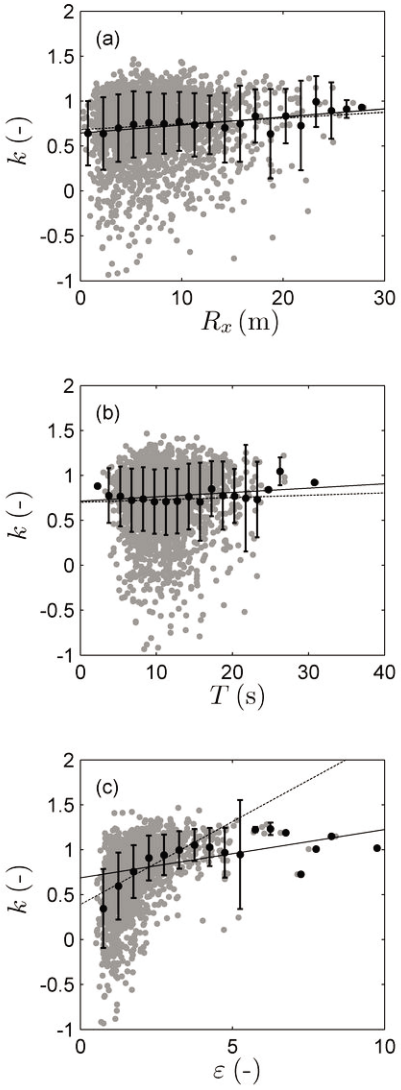

Figure 6. Comparison of individual k values with (a) R_x, (b) T, and (c) ε for all data. Data are binned corresponding to $R_x \pm 0.75$ m, $T \pm 0.75$ s, $\varepsilon \pm 0.25$. The mean and standard deviation of each bin range is shown (black circles) and values for individual data records (gray circles). Regression equations for binned data are shown by solid lines and correspond to the following equations: $k = (0.0089 \pm 0.0041)R_x + (0.65 \pm 0.068)$, $R^2 = 0.55$; $k = (0.0048 \pm 0.0051)T + (0.71 \pm 0.088)$, $R^2 = 0.20$; $k = (0.054 \pm 0.038)\ \varepsilon + (0.69 \pm 0.21)$, $R^2 = 0.38$. Regression equations for raw data are shown by dashed lines and correspond to the following equations: $k = (0.0064 \pm 0.0036)R_x + (0.68 \pm 0.030)$, $R^2 = 0.0050$; $k = (0.0026 \pm 0.0040)T + (0.70 \pm 0.045)$, $R^2 = 0.00067$; $k = (0.18 \pm 0.018)\ \varepsilon + (0.39 \pm 0.036)$, $R^2 = 0.19$.

wave height (H_o), the offshore average wave period (T_z), the beach slope in the swash zone ($\tan\beta_{sw}$), the Iribarren number (ξ) defined by

$$\xi = \frac{\tan\beta_{sw}}{\sqrt{H_o/L_o}}, \tag{12}$$

where $L_o = gT_z^2/2\pi$, and a swash interaction parameter ($\hat{T}$) defined by

$$\hat{T} = 2\left(\frac{2}{\pi}\right)^{1/4}\left(\frac{K^2 H_o}{gT^2\tan\beta_{sw}^2}\right)^{1/4}, \tag{13}$$

as given by *Brocchini and Baldock* [2008], which is a measure of the amount of interaction expected between monochromatic swashes for a given beach slope and offshore wave conditions. The difference between ε and ($\hat{T}$) arises through the use of the offshore wave height and period, rather than the swash amplitude and period, which are not independent of each other. Small values of $\hat{T}$ correspond to no swash interaction and values of $\hat{T}$ greater than or equal to 1 correspond to strong swash interaction. Usually $\hat{T}$ is greater than 1 except for long period swell on fairly steep beaches [*Brocchini and Baldock*, 2008]. In (13), K is an empirical factor that varies with beach type, but a value of $K \approx 0.6 - 0.8$ is representative of a wide range of beach types and wave conditions [*Stockdon et al.*, 2006]. It is useful to note that (13) is proportional to the inverse of $\sqrt{\xi}$, although it is derived independently. Mean values of k from Duck and NCEX were not correlated against the beach slope, the Iribarren number, or the swash interaction parameter because beach profiles were not collected at the same time as the video data used to generate the timestacks.

[24] $\overline{k}$ was found to be independent of H_o and T_z (not shown). Relationships between $\tan\beta_{sw}$, ξ and $\hat{T}$ are illustrated in Figure 7. A weak trend and low correlation was observed between $\overline{k}$ and $\tan\beta_{sw}$. However, this trend is due to the presence of one outlying data point (Cabarita, $\tan\beta_{sw} = 0.104$), and no trend and a further reduction in correlation was observed between $\overline{k}$ and $\tan\beta_{sw}$ when this point was removed from the analysis ($R^2 = 0.0073$; Figure 7a). Again, this lack of dependency is consistent with the theoretical basis of the model; the variation in patterns of flow reversal are a result of different inflow conditions for individual swash events and not strongly dependent on time-averaged offshore wave conditions or beach slope.

[25] Figure 7b shows the comparison of $\overline{k}$ with ξ. It is clear from Figure 7 and the previous histograms (Figure 4), that there is large variation of $\overline{k}$ within individual daily data sets as demonstrated by the large standard deviations. While a weak correlation of decreasing $\overline{k}$ with increasing ξ is apparent ($R^2 = 0.65$), as is the case with the relationship between $\overline{k}$ and $\tan\beta_{sw}$, this trend is again due to the presence of one outlying data point (Cabarita, $\xi = 0.74$) and no significant trend was observed between $\overline{k}$ and ξ when this point was removed from the regression analysis ($R^2 = 0.32$). Similarly, mean k values were also compared with $\hat{T}$ (Figure 7c). A weak trend of $\overline{k}$ increasing with increasing $\hat{T}$ occurred when all the data was considered ($R^2 = 0.65$), however, as with the trends between $\overline{k}$ and $\tan\beta_{sw}$ and $\overline{k}$ and ξ, no trend was observed when the one outlying data point was removed (Cabarita, $\hat{T} = 1.10$; $R^2 = 0.25$). Additionally, in both cases, as the standard deviations of $\overline{k}$ are large, any trends observed between daily $\overline{k}$ and ξ or $\hat{T}$ should be interpreted tentatively without further data (Figure 7).

4.3. Swash Interaction

[26] As indicated by Figure 6c, it appears that there is some influence of swash interaction on individual swash-

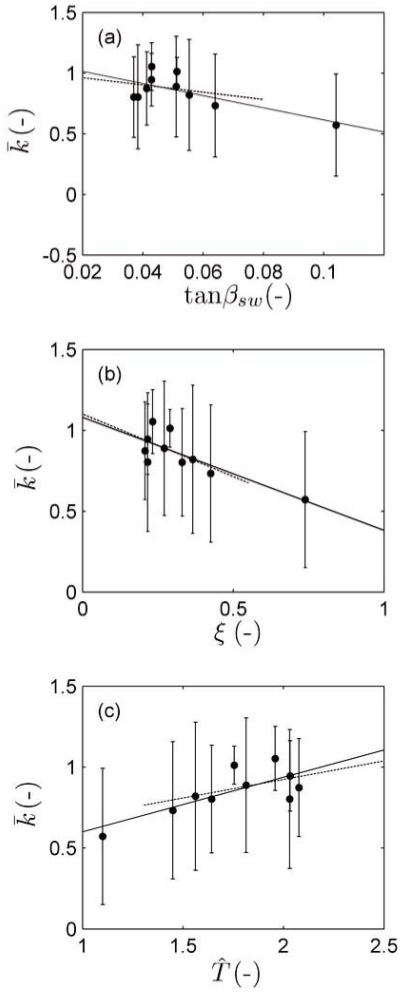

Figure 7. Comparison of mean k values (±standard deviation) (black circles) with (a) $\tan\beta_{sw}$, (b) ξ, and (c) $\hat{T}$ for each day of data excluding Duck and NCEX data. Regression equations are shown (solid lines) and correspond to the following equations: $k = (-4.56 \pm 3.91)\tan\beta_{sw} + (1.10 \pm 0.22)$, $R^2 = 0.47$; $k = (-0.70 \pm 0.42)\,\xi + (1.08 \pm 0.15)$, $R^2 = 0.65$; $k = (0.34 \pm 0.24)\,\hat{T} + (0.26 \pm 0.43)$, $R^2 = 0.56$. Regression lines are also shown (dashed lines) for the data without Cabarita ($\tan\beta_{sw} = 0.104$, $\xi = 0.74$, $\hat{T} = 1.10$) and correspond to the following equations: $k = (-0.91 \pm 9.49)\tan\beta_{sw} + (0.94 \pm 0.45)$, $R^2 = 0.0073$; $k = (-0.77 \pm 1.02)\,\xi + (1.10 \pm 0.30)$, $R^2 = 0.32$; $k = (0.23 \pm 0.36)\,\hat{T} + (0.46 \pm 0.66)$, $R^2 = 0.25$.

by-swash k values. To further investigate this, interactions between individual swashes were examined for the data set collected over a single day at Cabarita Beach, New South Wales, Australia. This data set was chosen as the images were high quality, k values could be obtained for a large proportion of the waves and therefore the data set has the largest number of k values for a near constant beach slope and offshore wave conditions. However, the data are still representative of the other beaches and the overall data set (see histograms in Figure 4). For each individual swash, the k value was plotted versus the rundown length (R_d) of the preceding swash (Figure 8). Here, the rundown length of the preceding swash is defined as the difference in the cross shore between the location of the maximum runup of the preceding swash and the location of the start of the swash event being considered (see Figure 3). This analysis demonstrates that the majority of swash events follow waves that have a preceding rundown greater than 1 m. Swash events preceded by a small rundown ($R_d < 1$ m) had mostly $k > 0.5$, and swash with small values of k tend not to occur following small rundown (i.e., few events plot in the lower left quadrant of Figure 8). Small or negative k values tend to occur predominantly following large preceding backwash ($R_d > 1$ m). However, a linear trend line fitted to the data shows only a weak correlation ($R^2 = 0.53$). Individual k values were also compared to the ratio of the runup length (R_x) and rundown length of the preceding wave (R_d), but no trend was observed in this comparison (not shown).

[27] To further investigate the dependence of k on the magnitude of the preceding rundown, k values were divided into two groups: those for swash with a small preceding rundown ($R_d < 1$ m) and those with a large preceding rundown ($R_d > 1$ m). Histograms of the two groups are shown in Figure 9. The k values for swash with small preceding rundowns, $R_d < 1$ m ($\overline{k} = 0.67$), were significantly larger than the k values for swash with large preceding rundown, $R_d \geq 1$ m ($\overline{k} = 0.54$; Figure 9; $\alpha = 0.01$; $t = 5.10$; d.f. = 554.30, $P < 10^{-6}$). This suggests that the swash zone boundary conditions and the period of inflow, as defined by k, are affected by interaction between individual swashes. Note that while the difference in $\overline{k}$ between these two populations is smaller than the RMSE arising from image resolution and the analysis method, there is no reason for any bias between

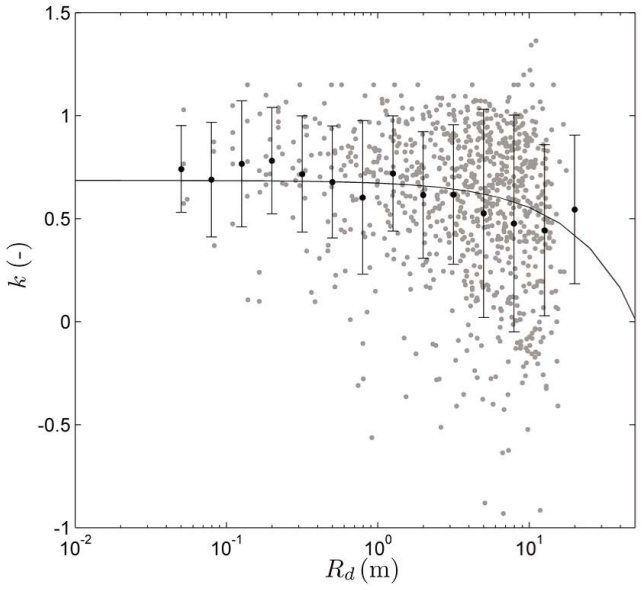

Figure 8. Comparison of k with the rundown length of the preceding wave (R_d) for individual waves at Cabarita. Data are binned corresponding to $R_d \pm 10^{0.1}$ m. The mean and standard deviation of each bin range is shown (black circles) and values for individual data records (gray circles). The regression equation for the binned data is shown by the solid line and corresponds to the following equation: $k = (-0.013 \pm 0.0075)R_d + (0.69 \pm 0.049)$, $R^2 = 0.53$.

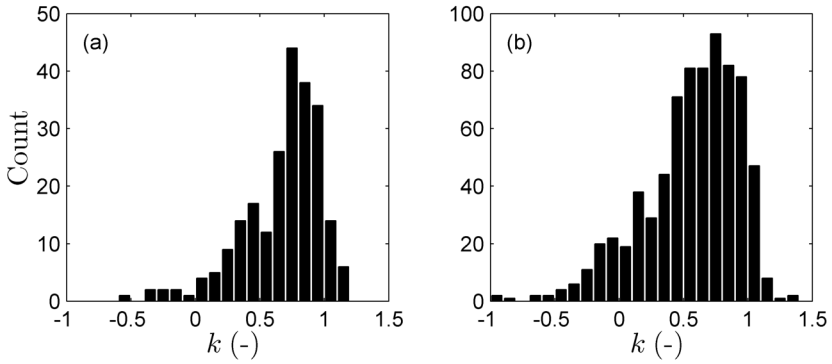

Figure 9. Histograms of k values for waves with preceding rundown of (a) $R_d < 1.0$ m ($n = 231$, $\overline{k} = 0.67$, $\sigma_k = 0.31$) and (b) $R_d \geq 1.0$ m ($n = 751$, $\overline{k} = 0.54$, $\sigma_k = 0.45$) for individual waves at Cabarita.

the two data sets, the populations are large, and therefore the difference in $\overline{k}$ is likely to be a result of the different preceding rundown lengths.

[28] The results shown in Figure 8 indicate that the swash can be divided into three types: (1) swash with small preceding rundown and therefore large k values, (2a) swash with large preceding rundown and small k values, and (2b) swash with large preceding rundown and large k values. In type (1), the preceding swash rundown is small or almost nonexistent and consequently very weak; therefore as the incoming bore overruns the preceding swash very little momentum is lost in counteracting the backwash. This ensures the incoming bore can sustain its inflow for a longer period of time leading to a later flow reversal time and therefore a large k value. An example of this type of swash is shown in Figure 5d.

[29] In the case of a large preceding rundown a wide range of k values is observed: swash types (2a) and (2b). In type (2a), the preceding swash has not finished its cycle and the incoming bore interacts strongly with the preceding backwash. This reduces the incoming bore velocity and the momentum of the fluid behind the bore front as the bore interacts with the strong offshore flow from the preceding swash. In this situation, the duration of the inflow into the swash zone is greatly reduced and flow reversal occurs early in the swash cycle, leading to a low value of k (e.g., Figure 5a). In some instances this situation can lead to the formation of a stationary hydraulic jump at the shoreline. This type of interaction is also described by *Hughes and Moseley* [2007] and referred to as strong wave-backwash interaction. Type (2b) differs from type (2a) in that the interaction between the preceding swash and the incoming bore is much weaker. The preceding swash has finished its swash cycle and the momentum of the incoming bore is not influenced by the preceding backwash. In this case, it is clear the interaction between swashes does not strongly impact on the inflow conditions and hence k. In this case, the asymmetry of the swash flow is determined solely by the inner surf zone conditions, notably the period for which the bore sustains the inflow into the swash zone at the position of the initial runup. This enables a wide range of k values to occur following a large preceding rundown. This situation is consistent with the *Guard and Baldock* [2007] and *Pritchard et al.* [2008] solutions, but inconsistent with the Shen-Meyer model where the swash conditions are independent of the bore conditions in the inner surf zone.

5. Discussion

[30] The observations and mean values for k shown here are consistent with *Hughes and Baldock* [2004] and *Houser and Barrett* [2010], who observed that flow reversal occurred on average after about 40% of the swash period (corresponding to $k \approx 0.8$–0.9) and ranged from one third of the swash period to over half of the swash period (corresponding to $0 < k < 1.2$), consistent with the remote sensing observations presented here. Such differences are unlikely to be a result of infiltration or friction, which predominantly affect the runup tip [*Hughes*, 1992; 1995; *Puleo and Holland*, 2001] and not the deeper flows at the seaward end of the swash zone.

[31] These results have significant implications for swash zone modeling. Incident bores that generate more sustained inflows to the swash zone (larger values of k) lead to deeper flow depths in the swash zone and a less asymmetric flow field. The mass and momentum flux are important in terms of predicting forces on structures in the runup zone, particularly for severe hazards such as the runup generated by tsunami bores, which has previously been estimated using the Shen-Meyer model [*Yeh*, 2007]. Longer and deeper inflows can carry more sediment, which influences the total quantity of sediment advected into the swash zone and the net transport of suspended sediment [*Pritchard and Hogg*, 2005; *Pritchard*, 2009]. A similar influence could be expected on the bed load transport. For example, Figure 10 illustrates how three time-averaged flow velocity parameters ($\overline{u^2}$, $\overline{u^3}$, and $\overline{u^4}$) that are widely used in typical sediment transport models vary with k. It is important to note that the flow velocity parameters are only shown for the range $-1 < k < 1.2$ as for $k > 1.2$ the model assumptions start to break down in the lower swash and a backwash bore forms such that the locus of $u = 0$ is not single valued across the swash zone (see section 4.1). As k increases, the net asymmetry reduces (moments reduce in magnitude), and this would be expected to significantly alter sediment transport patterns compared to the Shen-Meyer solution, which has a very asymmetric flow field. Accumulated over many swash events, this suggests that variations in the swash zone

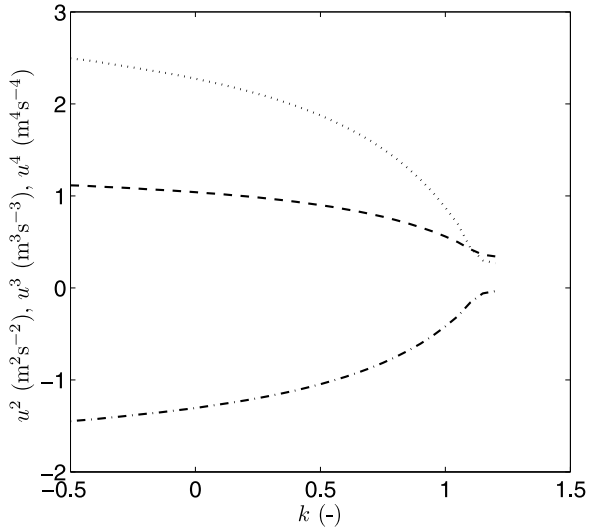

Figure 10. Variation of mean values of u^2 (dashed line), u^3 (dash-dotted line), and u^4 (dotted line) with k at $x = 0.2R_x$.

boundary conditions, and therefore the sediment fluxes into and across the swash zone, may be an important control on the net transport on the beach face. The observations of *Houser and Barrett* [2010] support this conjecture.

[32] The self-similarity of the swash solutions may enable this remote sensing technique to be combined with the numerical solutions to provide a hybrid model-data tool to derive further flow parameters in the swash zone. In the Guard-Baldock model, the complete dimensional hydrodynamic solution is determined solely by the runup amplitude, the beach face gradient and the value of k. Given that these three parameters can be measured quite accurately by remote sensing, it may be possible to infer other parameters, such as flow depths, flow velocities and net velocity asymmetry via a hybrid model-data tool. Nevertheless, improved resolution would be beneficial to reduce the errors in determining k values, and enabling a fully automatic approach to avoid any subjectivity. Model results calculated using observed k values and runup lengths would need to be compared to field measurements in the swash zone to verify the accuracy of the model. Further work is in progress on this issue. In conjunction with bathymetric data which can also be derived by remote sensing, this technique may provide a tool to correlate short and long-term changes in beach face morphology with the swash and inner surf zone conditions.

6. Conclusions

[33] Optical remote sensing provides an efficient and practical technique to measure of the variation in the time of flow reversal within the swash zone. Such observations can be used to quantify the duration and asymmetry of the inflow into the swash zone, which represent the controlling swash zone boundary conditions for individual swash events. These boundary conditions can be parameterized in terms of a single variable, k, from the *Guard and Baldock* [2007] model for swash hydrodynamics. Larger values of k represent more strongly sustained incident bores, which generate swash flows that are progressively deeper and less asymmetric. For real swash, derived k values occurred over a wide range, $-1 < k < 1.5$, with the majority of values in the range 0.5–1.2. This differs significantly from the analytical swash solution described by *Shen and Meyer* [1963] which corresponds to $k = 0$, indicating that the majority of real swashes have flows that are deeper and more symmetric than predicted by the Shen-Meyer model. This has implications for the sediment flux entering the swash zone and may be an important control on sediment transport on the beach face.

[34] **Acknowledgments.** The assistance of Ph.D. students at UQ on field trips is much appreciated. The authors are grateful to the Queensland government, Manly Hydraulics Laboratory, and the National Data Buoy Center, NOAA, for providing offshore wave and tide data. Useful and constructive review comments from the editor Thomas Herbers and two anonymous reviewers helped improve the manuscript. Funding from the ARC, DECCW (NSW state government), and DHI Australia is gratefully acknowledged.

References

Aagaard, T., and J. Holm (1989), Digitization of wave run-up using video records, *J. Coastal Res.*, *5*(3), 547–551.

Baldock, T. E. (2009), Discussion of "Measurement of wave-by-wave bed-levels in the swash zone" by Ian L. Turner, Paul E. Russell, Tony Butt, [Coastal Eng. 55(2008) 1237–1242], *Coastal Eng.*, *56*(3), 380–381, doi:10.1016/j.coastaleng.2008.12.002.

Baldock, T. E., and P. Holmes (1997), Swash hydrodynamics on a steep beach, in Coastal Dynamics '97, edited by E. B. Thornton, pp.784–793, Am. Soc. of Civ. Eng., New York.

Baldock, T. E., and P. Holmes (1999), Simulation and prediction of swash oscillations on a steep beach, *Coastal Eng.*, *36*(3), 219–242, doi:10.1016/S0378-3839(99)00011-3.

Baldock, T. E., and M. G. Hughes (2006), Field observations of instantaneous water slopes and horizontal pressure gradients in the swash-zone, *Cont. Shelf Res.*, *26*(5), 574–588, doi:10.1016/j.csr.2006.02.003.

Baldock, T. E., and D. Peiris (2010), Overtopping and run-up hazards induced by solitary waves and bores, in *The Tsunami Threat: Research and Technology*, edited by N.-A. Mörner, pp. 47–66, InTech, Rijeka, Croatia.

Baldock, T. E., M. G. Hughes, K. Day, and J. Louys (2005), Swash overtopping and sediment overwash on a truncated beach, *Coastal Eng.*, *52*(7), 633–645, doi:10.1016/j.coastaleng.2005.04.002.

Brocchini, M., and T. E. Baldock (2008), Recent advances in modeling swash zone dynamics: Influence of surf-swash interaction on nearshore hydrodynamics and morphodynamics, *Rev. Geophys.*, *46*, RG3003, doi:10.1029/2006RG000215.

Elfrink, B., and T. Baldock (2002), Hydrodynamics and sediment transport in the swash zone: A review and perspectives, *Coastal Eng.*, *45*(3–4), 149–167, doi:10.1016/S0378-3839(02)00032-7.

Guard, P. A., and T. E. Baldock (2007), The influence of seaward boundary conditions on swash zone hydrodynamics, *Coastal Eng.*, *54*(4), 321–331, doi:10.1016/j.coastaleng.2006.10.004.

Guza, R. T., and A. J. Bowen (1976), Resonant interaction for waves breaking on a beach, in *Proceedings of the Fifteenth Coastal Engineering Conference, Honolulu, HI, July 11-17, 1976*, pp. 560–579, Am. Soc. of Civ. Eng., New York.

Hibberd, S., and D. H. Peregrine (1979), Surf and run-up on a beach: A uniform bore, *J. Fluid Mech.*, *95*, 323–345, doi:10.1017/S002211207900149X.

Holland, K. T., and R. A. Holman (1993), The statistical distribution of swash maxima on natural beaches, *J. Geophys. Res.*, *98*(C6), 10,271–10,278, doi:10.1029/93JC00035.

Holland, K. T., and J. A. Puleo (2001), Variable swash motions associated with foreshore profile change, *J. Geophys. Res.*, *106*(C3), 4613–4623, doi:10.1029/1999JC000172.

Holman, R. A., and J. Stanley (2007), The history and technical capabilities of Argus, *Coastal Eng.*, *54*(6–7), 477–491, doi:10.1016/j.coastaleng.2007.01.003.

Houser, C., and G. Barrett (2010), Divergent behavior of the swash zone in response to different foreshore slopes and nearshore states, *Mar. Geol.*, *271*(1–2), 106–118, doi:10.1016/j.margeo.2010.01.015.

Hughes, M. G. (1992), Application of a non-linear shallow water theory to swash following bore collapse on a sandy beach, *J. Coastal Res.*, *8*(3), 562–578.

Hughes, M. G. (1995), Friction factors for wave uprush, *J. Coastal Res.*, *11*(4), 1089–1098.

Hughes, M. G., and T. E. Baldock (2004), Eulerian flow velocities in the swash zone: Field data and model predictions, *J. Geophys. Res.*, *109*, C08009, doi:10.1029/2003JC002213.

Hughes, M. G., and A. S. Moseley (2007), Hydrokinematic regions within the swash zone, *Cont. Shelf Res.*, *27*(15), 2000–2013, doi:10.1016/j.csr.2007.04.005.

Hughes, M. G., G. Masselink, and R. W. Brander (1997), Flow velocity and sediment transport in the swash zone of a steep beach, *Mar. Geol.*, *138*(1–2), 91–103, doi:10.1016/S0025-3227(97)00014-5.

Kemp, P. H. (1975), Wave asymmetry in the nearshore zone and breaker area, in *Nearshore Sediment Dynamics and Sedimentation*, edited by J. Hail and A. Carr, pp. 47–67, John Wiley, Hoboken, N. J.

Kobayashi, N., G. S. DeSilva, and K. D. Watson (1989), Wave transformation and swash oscillation on gentle and steep slopes, *J. Geophys. Res.*, *94*(C1), 951–966, doi:10.1029/JC094iC01p00951.

Larson, M., and N. C. Kraus (1994), Temporal and spatial scales of beach profile change, Duck, North Carolina, *Mar. Geol.*, *117*(1–4), 75–94, doi:10.1016/0025-3227(94)90007-8.

Lippmann, T. C., and R. A. Holman (1989), Quantification of sand bar morphology: A video technique based on wave dissipation, *J. Geophys. Res.*, *94*(C1), 995–1011, doi:10.1029/JC094iC01p00995.

Masselink, G., and M. Hughes (1998), Field investigation of sediment transport in the swash zone, *Cont. Shelf Res.*, *18*(10), 1179–1199, doi:10.1016/S0278-4343(98)00027-2.

Masselink, G., and J. A. Puleo (2006), Swash-zone morphodynamics, *Cont. Shelf Res.*, *26*(5), 661–680, doi:10.1016/j.csr.2006.01.015.

Miche, R. (1951), Le pouvoir réfléchissant des ouvrages maritimes exposés à l'action de la houle, *Ann. Ponts Chaussees*, *121*, 285–319.

Packwood, A. R. (1983), The influence of beach porosity on wave uprush and backwash, *Coastal Eng.*, *7*(1), 29–40, doi:10.106/0378-3839(83)90025-X.

Peregrine, D. H., and S. M. Williams (2001), Swash overtopping a truncated plane beach, *J. Fluid Mech.*, *440*, 391–399, doi:10.1017/S002211200100492X.

Power, H. E., M. Palmsten, R. A. Holman, and T. E. Baldock (2009), Remote sensing of swash zone boundary conditions using video and ARGUS, in *Proceedings of Coastal Dynamics 2009*, edited by M. Mizuguchi and S. Sato, pp. 1–11, Am. Soc. of Civ. Eng., New York.

Pritchard, D. (2009), Sediment transport under a swash event: The effect of boundary conditions, *Coastal Eng.*, *56*(9), 970–981, doi:10.1016/j.coastaleng.2009.06.004.

Pritchard, D., and A. J. Hogg (2005), On the transport of suspended sediment by a swash event on a plane beach, *Coastal Eng.*, *52*(1), 1–23, doi:10.1016/j.coastaleng.2004.08.002.

Pritchard, D., P. A. Guard, and T. E. Baldock (2008), An analytical model for bore-driven run-up, *J. Fluid Mech.*, *610*, 183–193.

Puleo, J. A., and K. T. Holland (2001), Estimating swash zone friction coefficients on a sandy beach, *Coastal Eng.*, *43*(1), 25–40, doi:10.1016/S0378-3839(01)00004-7.

Puleo, J. A., R. A. Beach, R. A. Holman, and J. S. Allen (2000), Swash zone sediment suspension and transport and the importance of bore-generated turbulence, *J. Geophys. Res.*, *105*(C7), 17,021–17,044, doi:10.1029/2000JC900024.

Puleo, J. A., K. T. Holland, N. G. Plant, D. N. Slinn, and D. M. Hanes (2003), Fluid acceleration effects on suspended sediment transport in the swash zone, *J. Geophys. Res.*, *108*(C11), 3350, doi:10.1029/2003JC001943.

Ranasinghe, R., G. Symonds, K. Black, and R. A. Holman (2004), Morphodynamics of intermediate beaches: A video imaging and numerical modelling study, *Coastal Eng.*, *51*(7), 629–655, doi:10.1016/j.coastaleng.2004.07.018.

Raubenheimer, B. (2002), Observations and predictions of fluid velocities in the surf and swash zone, *J. Geophys. Res.*, *107*(C11), 3190, doi:10.1029/2001JC001264.

Raubenheimer, B., R. T. Guza, S. Elgar, and N. Kobayashi (1995), Swash on a gently sloping beach, *J. Geophys. Res.*, *100*(C5), 8751–8760, doi:10.1029/95JC00232.

Shen, M. C., and R. E. Meyer (1963), Climb of a bore on a beach Part 3. Run-up, *J. Fluid Mech.*, *16*, 113–125, doi:10.1017/S0022112063000628.

Stockdon, H. F., and R. A. Holman (2000), Estimation of wave phase speed and nearshore bathymetry from video imagery, *J. Geophys. Res.*, *105*(C9), 22,015–22,033, doi:10.1029/1999JC000124.

Stockdon, H. F., R. A. Holman, P. A. Howd, and A. H. Sallenger (2006), Empirical parameterization of setup, swash, and runup, *Coastal Eng.*, *53*(7), 573–588, doi:10.1016/j.coastaleng.2005.12.005.

Turner, I. L., P. E. Russell, T. Butt, C. E. Blenkinsopp, and G. Masselink (2009), In-situ estimates of net sediment flux per swash: Reply to discussion by TE Baldock of "Measurement of wave-by-wave bed-levels in the swash zone", *Coastal Eng.*, *56*(9), 1009–1012, doi:10.1016/j.coastaleng.2009.06.001.

Waddell, E. (1976), Swash-groundwater-beach profile interactions, in *Beach and Nearshore Sediment*, *Spec. Publ. Ser.*, vol. 24, edited by R. A. Davis and R. L. Etherington, pp. 115–125, Soc. of Econ. and Paleontol. Mineral., Tulsa, Okla.

Wright, L. D., and A. D. Short (1984), Morphodynamic variability of surf zones and beaches: A synthesis, *Mar. Geol.*, *56*(1–4), 93–118, doi:10.1016/0025-3227(84)90008-2.

Yeh, H. (2007), Design tsunami forces for onshore structures, *J. Disaster Res.*, *2*(6), 531–536.

T. E. Baldock and H. E. Power, School of Civil Engineering, University of Queensland, Level 3, Room C312, Hawken Engineering Building, St Lucia, Qld 4072, Australia. (h.power@uq.edu.au)

R. A. Holman, College of Oceanic and Atmospheric Sciences, Oregon State University, 104 COAS Administration Bldg., Corvallis, OR 97331, USA.